

A new integrated methodology for the seismic assessment of urban areas

A. Greco^a, A. Pluchino^b, L. Barbarossa^a, G.Barreca^c, I. Calì^d, F. Martinico^a, A. Rapisarda^{b,d}

^a*Department of Civil Engineering and Architecture, University of Catania, via S.Sofia 64, Catania, Italy*

^b*Department of Physics and Astronomy “Ettore Majorana”, University of Catania, and INFN, via S.Sofia 64, Catania, Italy*

^c*Department of Biological, Geological and Environment Science, University of Catania, Corso Italia 57, Catania, Italy*

^d*Complexity Science Hub, Vienna, Austria*

Abstract

The analysis of the seismic vulnerability of urban centres has received a great attention in the last century, due to the progressive concentration of buildings in metropolitan areas. In order to estimate the seismic vulnerability of a densely populated urban area, it would in principle be necessary to develop in-depth analyses for predicting the dynamic behaviour of the individual buildings and their structural aggregation when subjected to the expected earthquake. Furthermore, in order to correctly estimate the soil structure interaction, reliable geological data for each site should be available. These detailed seismic analyses, however, are extremely cost-intensive, require great processing time and expertise judgement. The aim of the present study is to propose a new methodology able to combine information and tools coming from different scientific fields in order to reproduce the effects of a seismic input in urban areas, with known geological features, and to estimate the entity of the damages caused on existing buildings. In particular, we present an agent-based model of earthquake dynamics, based on the Self-Organized Criticality framework, in order to evaluate the effects of a sequence of seismic events on a certain large urban area during a given interval of time. The integration of GIS data sets, concerning both geological and urban information about the territory of Avola (Italy), allows performing a parametric study of these effects on a real context. The proposed new approach could be very useful in estimating the seismic vulnerability and defining planning strategies for seismic risk reduction in large urban areas.

Keywords: Seismic vulnerability; Urban areas; Gis; Numerical simulations; Self-organized Criticality

* Corresponding author. Tel.: 00390957382251;

E-mail address: annalisa.greco@unict.it

1. Introduction

The estimate of the seismic vulnerability of existing buildings has been extensively studied during the last 30 years at different scales, from the dimension of a single building to large urban areas. A reliable vulnerability evaluation for a single building requires expert analytical calculations and a deep knowledge of the geometry of the structure, of its mechanical properties and of the characteristic parameters of the foundation soil. It is evident that, due to the amount of data and resources involved in a rigorous assessment, it is economically unsustainable to extend to large urban context the detailed analyses developed on each single building. The change in scale involves therefore a reduction in the accuracy of the results. Nevertheless in order to define planning strategies for the reduction of seismic risk at urban scale, it is very important to be able to perform vulnerability assessments, based on simplified approaches and rapid processing.

Several procedures for a synthetic assessment of the seismic vulnerability of aggregates of buildings representing portions of urban areas have been presented in the scientific literature [1-6]. Seismic vulnerability assessments are referred to the expected seismic actions on the specific site, which can only be statistically presumed from previous recorded data and on the basis of the geological characteristic. Prescriptions of national codes make reference to the seismic hazard of the construction site that depends on the elastic response spectra related to the soil typology and to the ground acceleration with a predetermined probability of exceeding in the reference period of the construction. The seismic data related to the various construction sites are scaled according to the maximum acceleration expected on the ground, which, on the basis of past events, is related to the possibility of occurrence of a single seismic event of certain intensity. Anyway, large seismic events are often not isolated but are preceded and/or followed by a foreshock and an aftershock activity of variable intensity and duration (Omori Law) [7,8]. For example, the severe earthquake of magnitude 5.9 ML occurred in L'Aquila (Italy) on April 6 2009, at 3:32 a.m. (that caused more than 300 victims, 1,600 wounded and more than 10 billion euros of estimated damages), was the mainshock of an anomalous activity which started in December 2008 and lasted until 2012. In order to give an idea of the great number of shocks involved it is interesting to highlight that just in the year that followed the April 6 event, the Italian institute for geophysics and volcanology (www.ingv.it) reported that about 18,000 earthquakes occurred only across the area of the city of L'Aquila with different epicentres (256 events were registered only during the 48 hours immediately after the mainshock, 56 of them with a magnitude greater than 3 ML).

Apart from such catastrophic seismic scenarios, moderate ground activities are recorded every day all over the earth. When the intensity of the seismic input exceeds a minimum value, related to the structural characteristic of each building, the latter can suffer some damage, that in some cases could be difficult to identify but leads to a reduction of the seismic resistance of the structure. Therefore, not only severe ground motions constitute a danger for structures since damage can occur even for moderate seismic actions and a building can collapse after several small earthquakes due to incremental cumulative damage. In a seismic impact evaluation at regional or urban scale it would be very useful to have the possibility to estimate both the collapse scenario under severe earthquakes and the cumulative one caused by moderate and repetitive ground shakings. Of course the estimation of the seismic vulnerability of a given urban area strongly depends on the characteristics of the seismic input that can be predicted by means of modern techniques based on the available data.

One of these strategies has been developed in the context of the Self-Organized Criticality (SOC) theory. Introduced in 1987 by Bak, Tang and Wiesenfeld [10], SOC theory states that many large interactive systems observed in nature can self-organize into a "critical state" [11]. Once in this state, small perturbations may result in chain reactions, which can affect any number of elements within the system. In particular, the dissipative Olami-Feder-Christensen (OFC) model adopts the SOC hypothesis in order to reproduce the scale-invariant dynamics of real earthquakes on a regular square lattice, which mimics a portion of terrestrial crust [12]. When, after a given transient, the system enters into a critical state, the average earthquakes activity increases and events of any scale *may* occur. This is probably what happened between 2008 and 2012 in the territory of L'Aquila (Italy): the region entered into a critical state, and at that point the probability to experience a large earthquake, like that one of April 6 2009, was no more negligible, even if – as a consequence of the SOC dynamics – it would have been impossible to predict the exact moment in which that event would have been realized.

In this paper, by adopting the SOC framework of the OFC model, we propose an innovative methodology that integrates different tools and different sources of information in order to investigate the possible effects of a sequence of earthquakes on the urban settlement of a given geographical area. In particular, through an agent-based simulative approach, we show how it is possible to investigate the seismic vulnerability of that urban area, based on the structural characteristics of the existing buildings

and of the geological morphology of the territory, under the assumption that the crust below it would be set up into a critical state, i.e. that would experience a long sequence of earthquakes of any size with epicentres located in different parts of the considered territory.

This methodology is very general and it could be applied to areas of any size (being the SOC approach self-similar and scale invariant) but, in order to show its effectiveness, we have chosen as a case study the territory around Avola (Siracusa), a small city in the southeast part of Sicily, for which both urban and geological GIS data are available. This zone, from the point of view of the seismic risk, is very similar to the area around L'Aquila. This will allow us to calibrate the model in order to reproduce a damage scenario similar to that one observed in L'Aquila region in 2009. Then, we will address new seismic scenarios, before and into the critical state, and explore the possible effects of different earthquakes sequences on the existing buildings.

The paper is organized as follows. In Section 2, simple rules for estimating the seismic vulnerability of buildings in urban areas are described. In Section 3, the dynamics of the OFC model, and its adaptation to the classification adopted in the European Macroseismic Scale [13], are presented. In Section 4, the case study of Avola and the two GIS data sets (urban and geological) used in the paper are discussed. In Section 5 the OFC model is integrated with the datasets and calibrated through the comparison with real data about L'Aquila 2009 earthquakes [14-17]. Finally, in Section 6, the results of numerical simulations about several seismic scenarios involving the territory of Avola are presented, then some conclusions are drawn.

Table 1

Typologies	Building type	V _{min}	V _{max}
Masonry	Rubble stone and earth bricks	0.62	1.02
	Simple stone	0.46	1.02
	Massive stone	0.3	0.86
	Masonry with old bricks	0.46	1.02
	Masonry with r.c. floors	0.3	0.86
	Reinforced /confined masonry	0.14	0.7
Reinforced Concrete	Frame in r.c. (without E.R.D.)	0.3	1.02
	Frame in r.c. (moderate E.R.D.)	0.14	0.86
	Frame in r.c. (high E.R.D.)	-0.02	0.7
	Shear walls (without E.R.D.)	0.3	0.86
	Shear walls (moderate E.R.D.)	0.14	0.7
	Shear walls (high E.R.D.)	-0.02	0.54

2. Seismic vulnerability and damage evolution in existing buildings

The evaluation of the synthetic vulnerability value for each building in the urban area must take into account several parameters which among others consider the structural geometry, its age, the mechanical properties of the material, the quality of the construction and the geological characteristics of the site [18-20]. A reliable estimate of the seismic vulnerability of a single existing building needs therefore a significant amount of data even for a synthetic appraisal.

In absence of sufficient information, a representative vulnerability index related to the structural typology of each building can anyway be assumed following some approximate approaches presented in the scientific literature. An interesting proposal can be found in [18], where suitable ranges V_{\min} - V_{\max} for masonry and reinforced concrete buildings, furtherly classified according to the masonry typology and to the structural characteristic of the reinforced concrete structure, are presented. A summary of these ranges is reported in Table 1 and it can be observed that the vulnerability index V varies from a minimum value

$V_{\min} = -0.02$ for structures with high earthquake resistant design (E.R.D) to a maximum value $V_{\max} = 1.02$ in total absence of E.R.D. As explained in Section 4.1, these ranges will be adopted in the present paper to assign the “initial vulnerability” V_0 to each building, following also the information contained in the urban GIS data set. This vulnerability will be successively updated taking into account the damage produced by the seismic ground motion intensity (see later).

For the intensity of the seismic input, the classifications used in the European Macroseismic Scale (EMS) with the following 12 levels is here adopted: I. Not felt, II. Scarcely felt, III. Weak, IV. Largely observed, V. Strong, VI. Slightly damaging, VII. Damaging, VIII. Heavily damaging, IX. Destructive, X. Very destructive, XI. Devastating, XII. Completely devastating. This classification can be related to the most commonly adopted earthquake intensity scales as shown in [21]. In particular, the macroseismic intensity is considered as a continuous parameter in the range 1-12 evaluated taking also into account possible amplification effects with respect to a rigid soil conditions depending on the mechanical characteristics of the site. This means that the intensity of an earthquake, with a given seismic magnitude and a given released energy, can be perceived by the buildings differently in different areas according to corresponding geological typology.

A possible closed analytical function relating the expected damage μ_D to the seismic input has been proposed in [18]. In this study, such relation has been modified as follows:

$$\mu_D[I(c)] = 2.5 \left[1 + \tanh \left(\frac{I(c) + V - a}{bQ} \right) \right] \quad (1)$$

where $I(c)$ is the macroseismic intensity expressed as function of the parameter c , which represents the amplification value of the soil below the building (see next section), while V and Q are, respectively, building's vulnerability and ductility indexes. For the ductility index, the value $Q = 2.3$ has been assumed for masonry buildings, judged to be representative for buildings not specifically designed to have ductile behaviour. Most of the reinforced concrete buildings have been designed without taking into account the earthquake loadings, for this reason for all the r.c. building a low ductility index equal to $Q = 2.6$ has been assumed. It is worth to point out that increasing the value of Q , flattened curves are obtained, representative of more ductile behaviour, as less damage increase is observed for the same increase in seismic input. Finally, parameters a and b have to be chosen through a calibration analysis with the EMS-98, so that the most vulnerable building ($V_{\max}=1.02$, $Q=2.3$) results slightly damaged ($\mu_D=1$) for a single macroseismic event with intensity $I(\bar{c})$ of 6 and destroyed ($\mu_D \approx 5$) for an intensity $I(\bar{c})$ of 9, being \bar{c} the average value assumed by the amplification index c (see section 4.2). Following these prescriptions, we set $a=7.75$ and $b=0.5$.

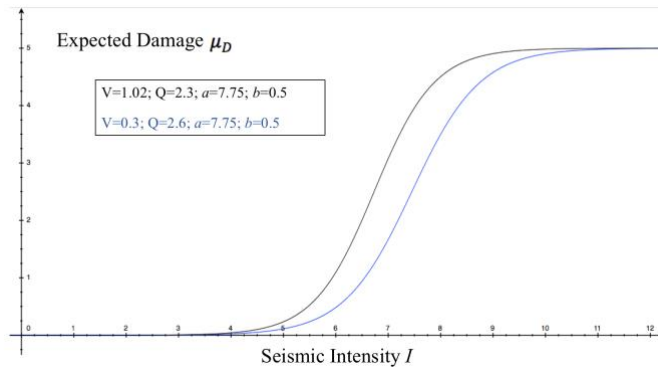


Figure 1. Example of expected damage vs seismic input I

In this paper, aiming at considering the damage cumulative process related to repetitive events, a simple original strategy for evaluating the reducing of structural performance associated to a sequence of earthquakes is presented. At a certain state, the total damage $\mu_D^{TOT} = \sum \mu_D$ for each building is defined as the sum of the damage parameters μ_D for each previous seismic event, evaluated according to equation (1). At the same time, the current vulnerability V_{new} is evaluated following the rule:

$$V_{new} = V_0 \left(1 + \frac{\mu_D^{TOT}}{5} \right) \quad (2)$$

where V_0 is the initial vulnerability (see Section 4.1). This means that subsequent earthquakes can progressively injure undamaged buildings, increasing their total damage μ_D^{TOT} (which starts from 0 at $t=0$) and changing their status according to the value of μ_D^{TOT} with respect to a parameter $1 < \gamma < 5$, chosen through a calibration with real data (see later). More in detail: when for a given building $1 \leq \mu_D^{TOT} < \gamma$, that building changes its status in “slightly damaged”; when $\gamma \leq \mu_D^{TOT} < 5$ the building is labelled as “highly damaged”; finally when $\mu_D^{TOT} \geq 5$, the status changes in “destroyed”.

The evaluation of the total damage for each building allows to globally visualize at the urban scale the areas with the same level of damage after each seismic input. As already pointed out, damage will successively proportionally modify the vulnerability of each structure which can therefore become progressively inadequate to stand successive ground motions.

The various parameters, and the procedure steps, introduced in this section will be reconsidered and further specified afterwards. Before this, more details are needed about the OFC model of earthquakes and the GIS datasets adopted in this paper.

3. OFC: a self-organized criticality model of earthquakes

The possibility of predicting earthquakes is a very old and debated one. This problem has stimulated many investigations along this direction in the last decades. One of the most realistic models, able to mimic the seismic activity dynamics, was proposed within the framework of Self-Organized Criticality (SOC) [10]. In particular, in ref. [21] it has been shown that it is possible to reproduce the statistical features of different earthquakes catalogues within a SOC context by considering a modification of the well-known Olami-Feder-Christensen (OFC) model.

The OFC model [12] can be viewed as a two-dimensional square lattice of side L with N sites. A seismogenic force F_i (seismic stress) acts on each site, which is connected to its four nearest neighbours. This force is a real number in the range $[0, F_{th}]$. To model a uniform tectonic loading dynamics as a function of time, all the forces are increased simultaneously and uniformly until one of them reaches the threshold value F_{th} (typically $F_{th} = 1$) and becomes “active”. At this point, the loading stops and an “earthquake” (avalanche) can start: the active node transfer a fraction α of its force to the four neighbours, which can in turn become active and pass the force to other neighbours, and so on and so forth. This simple dynamical rule can be written as

$$F_i \geq F_{th} \rightarrow \begin{cases} F_i \rightarrow 0 \\ F_{jj} \rightarrow F_{jj} + \alpha F_i \end{cases} \quad (3)$$

where “ jj ” denotes the set of nearest-neighbour nodes of i . The size S of a given earthquake, which represents the energy released by the seismic event, is given by the total number of sites activated during the avalanche dynamics. The parameter α controls the dissipation: the model is conservative if $\alpha = 0.25$, while it is dissipative for $\alpha < 0.25$.

The modification of the OFC model proposed in [21] did introduce long-range correlations in the original OFC lattice, therefore transforming it in a *small world* graph, a topological structure very

common for many real networks characterized by local clustering and a short average distance among its nodes [9]. Actually, the presence of just a few long-range links seems able to better simulate the features of real seismic faults, by creating shortcuts that connect sites (nodes) which otherwise would be much further apart. As it has been shown in [21], this kind of structure facilitates the system synchronization and produces both finite-size scaling and universal scaling exponents.

In this paper we adopt the small-world version of the dissipative OFC model, with $\alpha = 0.21$. In particular, the model is implemented on a regular grid network 40×40 with a total $N = 1600$ nodes, where the links are rewired at random with a small probability $p=0.02$ (typical of the small-world networks). Open boundary conditions are considered, i.e., $F_i = 0$ on the boundary nodes.

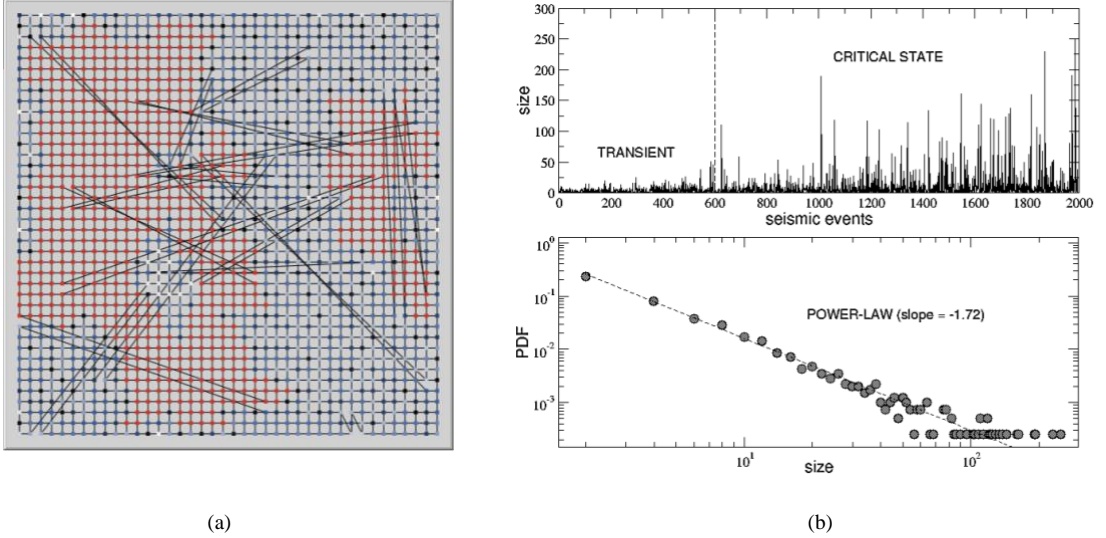


Figure 2. (a) The small-world lattice of the OFC model. Nodes in red represent the S sites activated by an earthquake of size S ; (b) The sequence of earthquakes' sizes in the transient and in the critical state (upper panel) with the corresponding probability distribution (lower panel), which is well fitted by a power-law curve with slope -1.72 (dashed line).

The resulting network is shown in Figure 2(a), where the brightness of each node (in grey-scale colour) is proportional to its level of seismic stress. In the top panel of Figure 2(b) the size S of 2000 subsequent earthquakes during a typical run of the OFC dynamics is plotted. After a transient of about 600 events, where the maximum size involves less than 5% of the entire lattice, the system enters into a critical state, where the average size of the earthquakes starts to increase and large events, involving a great number of nodes, have a non-zero probability of occurrence. The nodes activated during one of these large events are coloured in red in Figure 2(a). The presence of criticality in the earthquakes' sequence is revealed by a power-law probability distribution function (pdf) of the size S , i.e. of the released energy, which appears as a straight line in the log-log plot shown in the bottom panel of Figure 2(b). The power-law is also the signature of a scale-invariant behaviour of the shocks, meaning that the size distribution of the avalanches has a self-similar structure at all spatial scales.

In order to adapt the OFC model output to the classification used in the European Macroseismic Scale (EMS-98), one needs to transform the size S of a given earthquake into the corresponding intensity I , which – as already said – presents 12 different possible levels. The first step is to calculate the magnitude M of the earthquake, which is usually defined as the natural logarithm of the released energy: $M = \ln S$ (being the energy released an exponential function of the magnitude: $S = e^M$). Then, the magnitude can be transformed in the macroseismic intensity through the following empirical relation: $I(M) = 1.71 M - 1.02$, obtained through a comparison between the magnitude scale and the EMS-98 one. For example, the first noticeable peak in the sequence shown in the top panel of Figure 2(b) has a size $S = 267$ nodes, a

magnitude $M = 5.6$ and an intensity $I(M) = 8.53$. Finally, due to the geological characteristic of the soil, the final intensity perceived in a given area will be:

$$I(M,c) = I(M) + c \quad (4)$$

where c is the previously introduced amplification index characteristic of that area (see section 4.2).

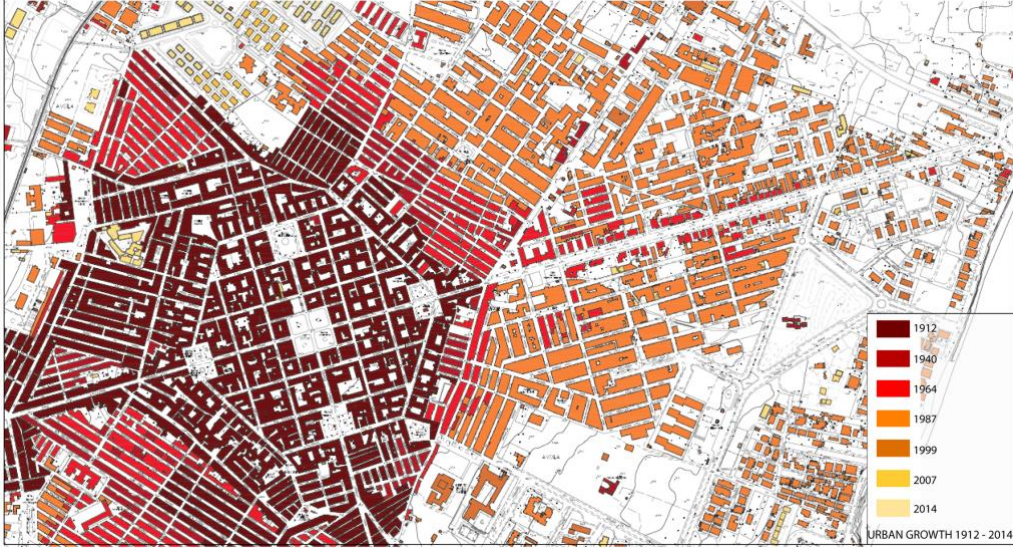


Figure 3. City of Avola - Urban Growth map

4. The case study of Avola

In this section, the case study of Avola is introduced and the integration of the OFC model with two, urban and geological, GIS datasets is discussed. It is worth to notice that this has been considered as an example finalized to show the effectiveness of the proposed procedure in providing an estimation of seismic vulnerability of a given urban area.

The city of Avola (31576 inhabitants in 2016) is located along the south-east coast of Sicily, the so-called Val di Noto, thirty kilometres south of Siracusa. According to the Italian seismic hazard map (<http://zonesismiche.mi.ingv.it>), this area is very similar to the one around L'Aquila. It was completely destroyed in 1693 by a major earthquake that hit South-eastern Sicily, causing thousands of victims. More than 45 cities were destroyed or severely damaged. This catastrophic event caused a complete change in the structure of the entire 'Val di Noto' area, where a number of cities were rebuilt in new sites, closer to the coast.

After the earthquake, also the city of Avola was rebuilt in a new site according to a completely new layout in the coastal plain, one kilometre far from the coastline. The urban structure is characterized by a grid of perpendicular streets within an hexagonal perimeter. A large main square with nearby minor ones marks the heart of the town, according to a design inspired by the ideal cities plans from the Renaissance. Until the end of 19th century, the urban growth around the early urban core was influenced by the hexagonal shape of the settlement (Fig. 3), made by concentric blocks, somewhere irregular. The pattern based on compact and regular rectangular blocks repeats the model of the agro towns founded in Sicily from 15th to 17th century, especially during the Spanish domination. At the beginning, the regular grids were aligned to the sides of the hexagon and after their layout was oriented by the grid of existing long

distance and rural roads. This phase addressed the relevant demand of urban growth between the 1940 and 1960.

Between 1970 and 1990, along with the urban core development, two new processes moulded the shape of the settlement. The first was the development of extensive subdivisions with detached single family holiday houses along the coastline, a phenomenon that overwhelmed the fragile coastal ecosystem, the second one was the low-density urbanization of peri-urban and rural areas where a considerable number of small and medium size houses have been built by the land owners for week-end or seasonal usage. Recently the, urban growth processes have been governed by poor quality urban plans that gives marginal attention to agricultural land protection and sustainability. The result are the new medium density settlements, developed close to the town centre, following an awkward interpretation of the modernist planning models [23].

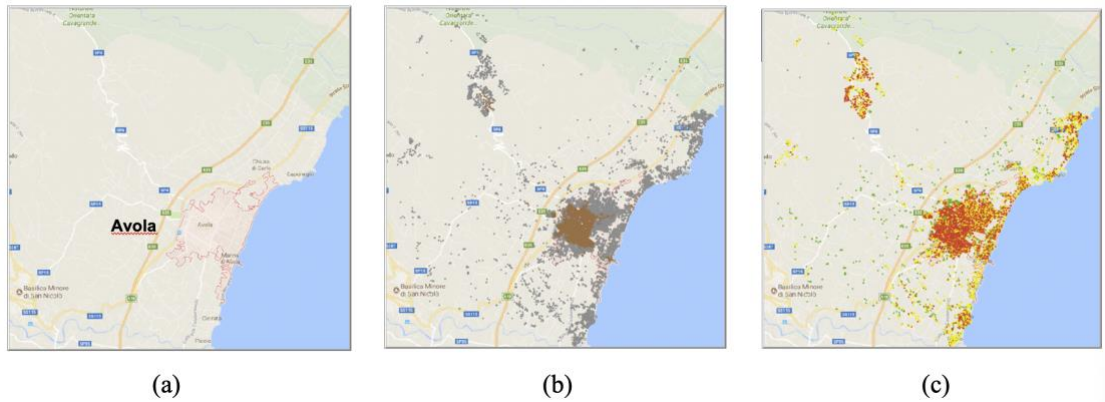


Figure 4. (a) Territory of Avola; (b) Gis dataset: Masonry (brown) and reinforced concrete (grey) buildings; (c) Low (green), medium (yellow) and high (red) vulnerability buildings.

4.1. Description of the urban GIS dataset

During the new city masterplan design process, carried out from 2013 to 2016, data were collected, digitized and georeferenced, to analyse urban growth of the city. The study was based on all the historical cartographies available, it produced a map representing the growth of Avola settlement from the foundation in the early 18th century, from 2015.

Historical cartographies of urban fabric were overlaid with new official cartography, released by Urban Planning Department of the Regional Government, in order to obtain an historical dating of the entire built up area. As a result, urban growth had been quantified and mapped measuring the built-up changes corresponding to seven dates (1912, 1940, 1964, 1987, 1999, 2007, 2014).

The resulting urban growth map gives for each building of the urban fabric the date in which it is present in the corresponding map. This allows an estimate of the period of construction for each building. In addition, using the data (height and surface) derived from the official vectorial cartography, the volume of each building of the urban fabric has been computed by using standard GIS functions. As a result, every building in Avola has been characterized by its volume, height and construction date attributes in the GIS dataset. In addition, the dataset includes the same information for other buildings scattered in the territory around Avola. In particular, a square area with a side length of 10,5 Km has been considered, as shown in Figure 4(a).

The total number of buildings in this area is $N_B=17477$. Depending on their period of construction, all the buildings were classified in two main categories, reported in Figure 4(b) with different colours: masonry

buildings (before 1965, in brown) and reinforced concrete buildings (after 1965, in grey). Buildings of the first category will present a ductility $Q=2.3$, while those of the second category will have $Q=2.6$. Then, crossing the construction information with data about the ratio $R=H/L$ between height H and base side L , an initial vulnerability index V_0 – see equation (2) – has been assigned to each building following the prescriptions of Table 1: in Figure 4(c) we represent in green buildings with low vulnerability ($-0.02 < V_0 < 0.3$), in yellow those with medium vulnerability ($0.3 < V_0 < 0.65$) and in red those with high vulnerability ($0.65 < V_0 < 1.02$).

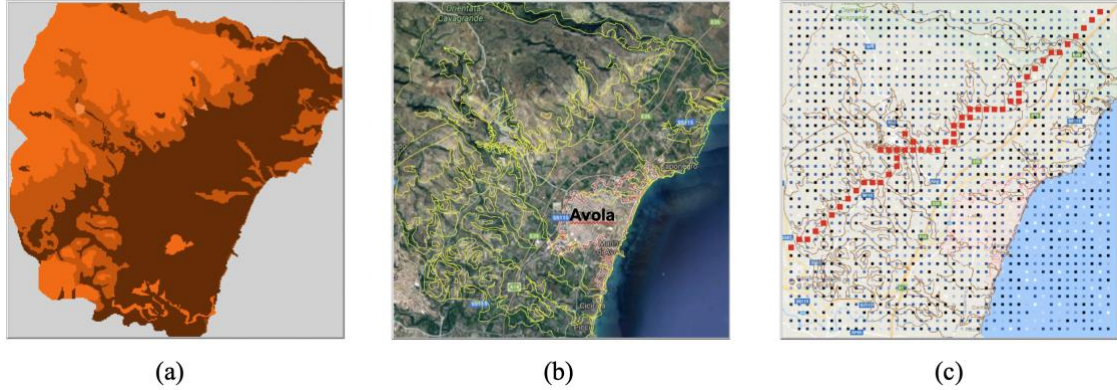


Figure 5. (a) Geological GIS dataset; (b) Site-amplification map of the territory of Avola; (c) OFC lattice: red nodes along the fault have a greater probability to be activated and to trigger an earthquake.

4.2 Geological framework and GIS dataset

During the new city masterplan design process, carried out from 2013 to 2016, a large amount of geological data was collected, digitized and properly stored within a geo-referenced digital data set. Among many thematic maps, the “geology” layer was used in the present analysis to empirically predict stratigraphic site-amplification (expressed by the previously introduced c index), a factor which is primarily controlled by the thickness of soft sediments above a rigid substratum – see Figure 5(a). This stratigraphic configuration (soft/rigid) is quite common in the sector where the urban settlement of Avola extends since it consists of an ancient fluvial to marine depositional system discharging soft-sediments (clays, sands and conglomerates) which accumulated above a pre-existing (today buried) topographic surface modelled on carbonate (rigid) rocks.

The carbonate top-surface was reconstructed within the GIS environment by interpolating (Spline) the elevation of the top of the “rigid” geological formations, a point-value obtained from the consultation of a numbers of wells (and associated stratigraphic logs) available for the area. Thickness for the soft-sediments was therefore derived by subtracting the modern topographic surface (2x2m cell size DTM) from the interpolated carbonate top-surface. Numerical values were then spatially joined to the polygon features describing the areal distribution of the outcropping geological formations. Since thickness can amplify or dampen the amplitude of seismic waves, a degree of amplification (medium-low, medium, medium-high and high) was associated (according to the thickness) to each geological formation, producing a new thematic map – see Figure 5(b), where the different geological areas are delimited by yellow lines tracked over a satellite image of the considered territory. With reference to equation (4), expressing the earthquake intensity perceived by a given area, the following values for the amplification

index c can be assigned: $c = -0.5$ (for geological sites with a medium-low amplification), $c = 0$ (medium amplification), $c = 0.5$ (medium-high amplification), $c = 1$ (high amplification).

The territory of Avola is also sliced by a NE-SW trending tectonic structure which has been classified as an active and capable fault by ISPRA (Istituto Superiore per la Protezione e la Ricerca Ambientale) and added in the ITHACA (ITaly HAZard from CApable faults) data set (<http://sgi2.isprambiente.it/ithacaweb/viewer>). The tectonic structure consists of a 15 km-long, SE-dipping extensional fault located less than 3 km from the Avola city-center and separating the Avola mountains from the coastal plain with a 300 m-high morphological scarp. Although its geometry at depth is still unknown, its occurrence gave us useful information to construct a reality-based lattice taking into account that the triggering of an earthquake is likely by approaching the fault plane.

In Figure 5(c) the OFC small-world lattice, already shown in Figure 2(a), is superimposed on the considered square map of the territory of Avola (links are hidden in the figure, only nodes are visible). In order to incorporate the tectonic information in the OFC model, each node carries the value of the amplification index c of the area immediately around it. Moreover, nodes along the fault (in red) also carry a seismic stress F_i which – at variance with the other nodes – will take values in the interval $[0.2, F_{th}]$; therefore these nodes will have a greater probability to be activated by the OFC dynamics and to trigger an earthquake.

5. Calibration of the model

As already said, the target of this study is to propose an innovative methodology for the evaluation, through agent-based simulations, the impact of a sequence of earthquakes on the vulnerability of the buildings present in the territory of Avola, under the assumption that this area, like the L'Aquila territory in 2009, is in a critical state. Before going forward with the analysis of new seismic scenarios, the model needs to be calibrated in order to choose the optimal values of the tuning parameters.

For this purpose, due to the similarity (in terms of seismic risk) of the two territories, the idea is to reproduce, with a certain degree of approximation, the seismic scenario of L'Aquila in 2009 and to calibrate the model parameters by comparing the simulated effects of earthquakes on Avola's buildings with the real effects documented by some technical reports realized after the most destructive earthquakes in L'Aquila [17]. In this respect, we consider the most intense period of seismic activity, from 01/04/2009 to 10/04/2009. During these 10 days hundreds of earthquakes occurred within the L'Aquila's territory (100 per day, in average), most of them of magnitude between 3 and 4 ML, with a peak event of 5.9 ML (on 06/04) and other three events above 5 ML (between 06/04 and 10/04). The effects of this impressive seismic sequence on the urban structure of L'Aquila and on the immediately surrounding areas were evaluated in 17% of heavily damaged buildings and in 24% of destroyed ones.

In order to reproduce a similar scenario with our simulations in the context of the considered case study of Avola, the OFC model introduced in section 3 has been finally integrated with both the urban and the geological GIS datasets presented in the previous section, as shown in Figure 6(a). The distance between two rows or two columns of the usual small-world lattice with $N=1600$ nodes corresponds to about 250 meters on the map. Running the OFC model, after a transient of 600 relatively small events the system enters into the critical state; then, a sequence of shocks with any size do occur. In analogy with L'Aquila scenario, we will consider a time window of 10 days, corresponding (by assuming 100 shocks per day) to a sequence of $N_S=1000$ seismic events, whose size (for a trial simulation) is reported in the top panel of Figure 6(b). As explained in section 3, each size S can be first translated in the corresponding magnitude M , then the latter can be further transformed in the macroseismic intensity scale $I(M)$: these last two quantities, for the same initial sequence, are reported, respectively, in the middle and bottom panels of Figure 6(b). The data about magnitude allow to appreciate the presence, in the considered sequence within

the critical state, of many events with $3 < M < 4$, eight events with $4 < M < 5$ mostly concentrated in the last five days and a couple of events with $M > 5$: the first one of 5.6 ML at day 6th and the second one of 5.98 ML at day 9th. We can therefore assume this sequence as a good proxy of what really happened in the 10 days between 01/04/2009 and 10/04/2009 in L'Aquila territory.

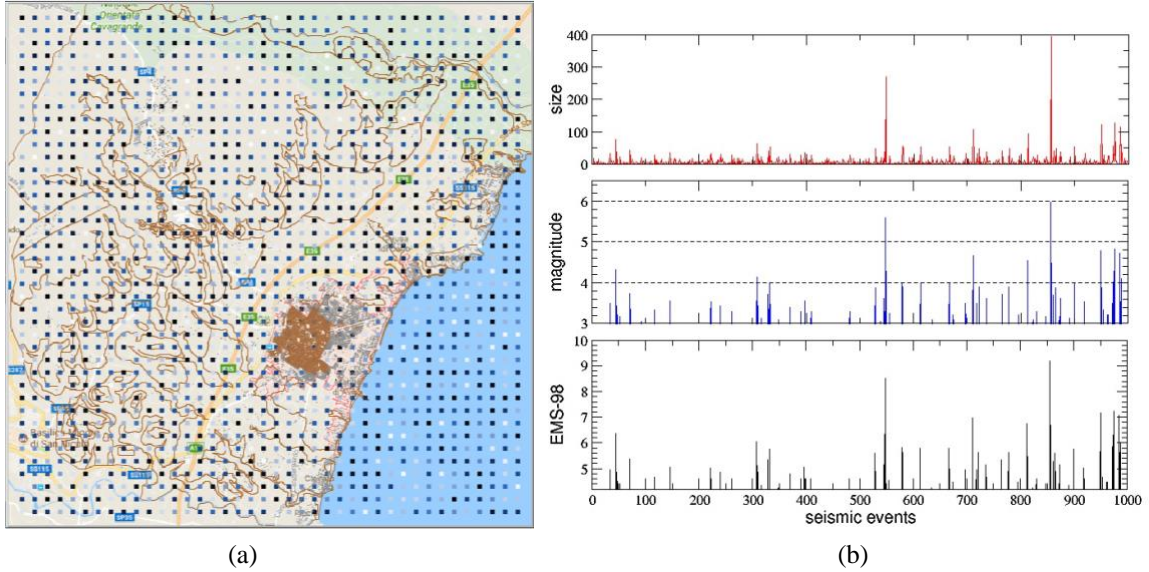


Figure 6. (a) OFC model integrated with both the urban and geological GIS datasets for the Avola territory; (b) The sequence of 1000 earthquakes (size, magnitude and EMS-98 intensity) which reproduce the seismic scenario of L'Aquila in 2009

Let us describe, now, how these seismic events interact, into the simulation environment, with the buildings present in the Avola territory. In correspondence of a single earthquake of size S (and magnitude $M = \ln S$), each one of the S activated nodes of the lattice (see Section 3) transfers a seismic stress of the corresponding intensity $I(M, c)$ to a certain fraction f_B of buildings, randomly chosen among all those included in a circle of radius $R = 250 \text{ mt} \cdot \sqrt{2/2} = 176.8 \text{ mt}$ around the active node (of course, buildings included in intersections among different circles are taken into account only ones). Notice that the intensity $I(M, c)$ perceived by these buildings will depend not only on the magnitude M but also on the value of the amplification index c carried by the particular node which transfer to them the seismic stress. Therefore, as already explained in Section 2, the final result of each simulated earthquake on the buildings, will be the one of injuring them, by increasing their total cumulated damage μ_D^{TOT} of a quantity μ_D which depends, according to Equation (1), on their ductility and vulnerability, but which also enhances, in turn, the vulnerability itself according to Equation (2).

During the considered simulation, being the buildings subjected to a sequence of N_S earthquakes, they can progressively change their status according to the value of μ_D^{TOT} with respect to the threshold parameter γ : when $1 \leq \mu_D^{TOT} < \gamma$ a given building changes its status in “slightly damaged”, when $\gamma \leq \mu_D^{TOT} < 5$ the same building results to be “highly damaged”, and when $\mu_D^{TOT} \geq 5$ the status becomes “destroyed”. At the end of the simulation, the percentages P_{HDB} and P_{DEB} of, respectively, highly damaged and destroyed buildings over the total $N_B = 17477$ will be considered as a good indicator of the global response of the territory of Avola to the seismic inputs. But of course these percentages will depend on the choice of the threshold parameter γ and of the fraction f_B of randomly chosen buildings in the neighborhood of each active node of the lattice during an earthquake. By performing several runs of the same sequence of $N_S = 1000$ seismic events, with different choices of these two parameters, and comparing

the outputs with the expected ones coming from real data about damages in L'Aquila 2009 scenario, we found that the values $\gamma = 3.17$ e $f_B = 0.35$ were able to produce the best results showed in Table 2.

Table 2

	P _{HDB} (Heavily Damaged Buildings)	P _{DEB} (Destroyed Buildings)
AVOLA (simulations)	16.8%	24.3%
L'AQUILA 2009 (real data)	17%	24%

In Table 3, details about the process of progressive damaging of the buildings when the system is in the critical state, for a simulation of the sequence showed in Figure 6(b) and with this choice of the parameters, are reported. In particular, for each seismic event occurred during the considered period of 10 days, next to the magnitude and the corresponding EMS-98 intensity $I(M)$, the corresponding number of heavily damaged and destroyed buildings are reported. Notice that only earthquakes with magnitude greater than 3 are shown in the Table.

In order to better appreciate the progression of damages, the same data about buildings are plotted in the top panel of Figure 7(a), while in the bottom panel the sequence of the magnitude of seismic events (already reported in Figure 6(b)) is also plotted for comparison. It is evident that the largest increments in the number of damages occur in correspondence with the two main shocks of magnitude 5.6 ML and 5.98 ML respectively. Finally, in Figure 7(b) the colour map of damages for the portion of territory strictly around Avola is shown: undamaged or slightly damaged buildings are coloured in green, while heavily damaged and destroyed ones are coloured in yellow and red, respectively. Of course, since all the desired details about each single damaged or destroyed building are known (size, data of construction, vulnerability, typology, geological features of the edification soil, etc.), this methodology would also allow to perform any kind of statistical analysis of the final damage scenario.

In the next section we will address this point in the context of new hypothetical seismic scenarios involving the territory of Avola.

Table 3

"M = 3.5 EMS98 = 4.95 damaged = 0 destroyed = 0"	"*****"	"*****"
"M = 4.32 EMS98 = 6.35 damaged = 1 destroyed = 0"	"M = 3.3 EMS98 = 4.61 damaged = 10 destroyed = 2"	"M = 4.55 EMS98 = 6.76 damaged = 1243 destroyed = 727"
"M = 3.43 EMS98 = 4.85 damaged = 1 destroyed = 0"	"M = 3.5 EMS98 = 4.95 damaged = 10 destroyed = 2"	"M = 3.18 EMS98 = 4.41 damaged = 1243 destroyed = 727"
"M = 3.18 EMS98 = 4.41 damaged = 1 destroyed = 0"	"End day 5"	"M = 3.3 EMS98 = 4.61 damaged = 1239 destroyed = 731"
"M = 3.74 EMS98 = 5.36 damaged = 1 destroyed = 0"	"*****"	"M = 3.18 EMS98 = 4.41 damaged = 1239 destroyed = 731"
"M = 3.04 EMS98 = 4.18 damaged = 1 destroyed = 0"	"M = 3.85 EMS98 = 5.56 damaged = 14 destroyed = 3"	"M = 3.4 EMS98 = 4.79 damaged = 1239 destroyed = 731"
"End day 1"	"M = 3.09 EMS98 = 4.26 damaged = 14 destroyed = 3"	"M = 5.98 EMS98 = 9.2 damaged = 2938 destroyed = 4081"
"*****"	"M = 4.13 EMS98 = 6.03 damaged = 14 destroyed = 3"	"M = 3.66 EMS98 = 5.24 damaged = 2936 destroyed = 4083"
"M = 3.33 EMS98 = 4.67 damaged = 1 destroyed = 0"	"M = 3.61 EMS98 = 5.15 damaged = 15 destroyed = 4"	"M = 3.87 EMS98 = 5.59 damaged = 2937 destroyed = 4084"
"M = 3.56 EMS98 = 5.05 damaged = 1 destroyed = 0"	"M = 5.6 EMS98 = 8.54 damaged = 1280 destroyed = 602"	"M = 3.18 EMS98 = 4.41 damaged = 2937 destroyed = 4084"
"End day 2"	"M = 3.26 EMS98 = 4.54 damaged = 1280 destroyed = 602"	"M = 3.61 EMS98 = 5.15 damaged = 2940 destroyed = 4086"
"*****"	"M = 3.81 EMS98 = 5.48 damaged = 1280 destroyed = 602"	"M = 3.14 EMS98 = 4.34 damaged = 2940 destroyed = 4086"
"M = 3.22 EMS98 = 4.48 damaged = 1 destroyed = 0"	"End day 6"	"M = 3.97 EMS98 = 5.76 damaged = 2906 destroyed = 4125"
"M = 3.53 EMS98 = 5 damaged = 1 destroyed = 0"	"*****"	"End day 9"
"M = 3.43 EMS98 = 4.85 damaged = 1 destroyed = 0"	"M = 3.99 EMS98 = 5.79 damaged = 1294 destroyed = 610"	"*****"
"M = 3.3 EMS98 = 4.61 damaged = 1 destroyed = 0"	"M = 3.09 EMS98 = 4.26 damaged = 1263 destroyed = 641"	"M = 3.53 EMS98 = 5 damaged = 2875 destroyed = 4156"
"End day 3"	"M = 3.99 EMS98 = 5.79 damaged = 1263 destroyed = 641"	"M = 4.84 EMS98 = 7.24 damaged = 2933 destroyed = 4164"
"*****"	"M = 3.22 EMS98 = 4.48 damaged = 1263 destroyed = 641"	"M = 3.33 EMS98 = 4.67 damaged = 2931 destroyed = 4166"
"M = 3.14 EMS98 = 4.34 damaged = 1 destroyed = 0"	"M = 3.5 EMS98 = 4.95 damaged = 1255 destroyed = 649"	"M = 3.09 EMS98 = 4.26 damaged = 2931 destroyed = 4166"
"M = 4.13 EMS98 = 6.03 damaged = 3 destroyed = 2"	"End day 7"	"M = 3.22 EMS98 = 4.48 damaged = 2931 destroyed = 4166"
"M = 3.43 EMS98 = 4.85 damaged = 3 destroyed = 2"	"*****"	"M = 3.83 EMS98 = 5.52 damaged = 2931 destroyed = 4166"
"M = 3.14 EMS98 = 4.34 damaged = 3 destroyed = 2"	"M = 4.67 EMS98 = 6.96 damaged = 1259 destroyed = 653"	"M = 3.58 EMS98 = 5.1 damaged = 2931 destroyed = 4166"
"M = 3.71 EMS98 = 5.32 damaged = 5 destroyed = 2"	"M = 3.5 EMS98 = 4.95 damaged = 1259 destroyed = 653"	"M = 4.84 EMS98 = 7.25 damaged = 2950 destroyed = 4198"
"M = 3.97 EMS98 = 5.76 damaged = 6 destroyed = 2"	"M = 3.87 EMS98 = 5.59 damaged = 1263 destroyed = 654"	"M = 4.74 EMS98 = 7.07 damaged = 2943 destroyed = 4255"
"M = 3.09 EMS98 = 4.26 damaged = 6 destroyed = 2"	"M = 3.81 EMS98 = 5.48 damaged = 1263 destroyed = 654"	"M = 3.33 EMS98 = 4.67 damaged = 2943 destroyed = 4255"
"M = 3.4 EMS98 = 4.79 damaged = 10 destroyed = 2"	"M = 3.61 EMS98 = 5.15 damaged = 1265 destroyed = 655"	"End day 10"
"M = 3.56 EMS98 = 5.05 damaged = 10 destroyed = 2"	"M = 3.89 EMS98 = 5.63 damaged = 1222 destroyed = 699"	"*****"
"End day 4"	"M = 3.22 EMS98 = 4.48 damaged = 1222 destroyed = 699"	
	"End day 8"	

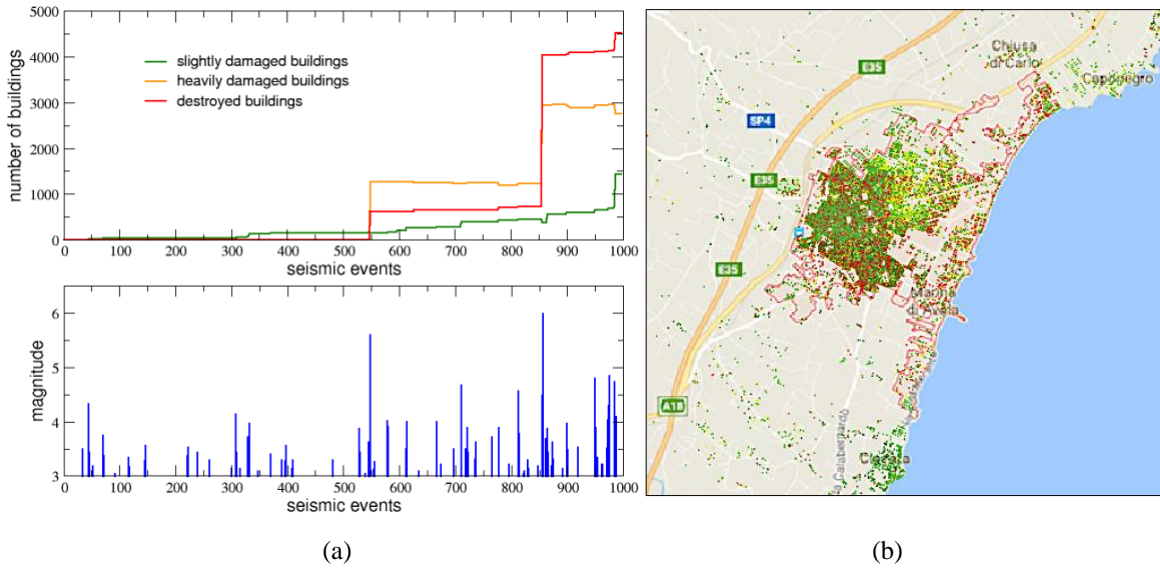


Figure 7. (a) Top panel: number of (slightly or heavily) damaged and destroyed buildings as function of seismic events; Bottom panel: magnitude of seismic events; (b) Picture of the damages after the entire sequence of seismic events for a smaller portion of territory just around Avola: undamaged or slightly damaged buildings are in green, heavily damaged ones in yellow and destroyed ones in red.

6. New Seismic Scenarios: numerical results

6.1 Evaluation of damages into shifted time windows with increasing seismic activity

Once calibrated the model and fixed the control parameters, in this subsection we first test the potentiality of our model by considering a new sequence of 2000 earthquakes occurring in the Avola's territory, which starts out of the critical state and reaches criticality after a transient of 600 events. In particular, we consider a moving time window including 1000 events (corresponding, as usual, to about 10 days), starting at $t=0$ and shifting on the right with five consecutive steps of 200 events each. In Figure 8 the complete sequence is shown, together with the six subsequent positions of the moving window which have been taken into account. For each event, the corresponding magnitude is reported on the y-axis and a horizontal dashed line helps the eye in recognizing events with $ML > 3$.

In what follows, the damage scenarios corresponding to each one of the six windows will be analyzed, in order to evaluate to what extent the seismic effects on buildings of the urban and peri-urban area of Avola are sensitive to a progressive increase in the earthquake intensity. For this purpose, in Figure 9 the behavior of the number of both (slightly or heavily) damaged and destroyed buildings is reported for each moving window (top panels), together with the magnitude of the corresponding events (bottom panels). For sake of clarity, among the total of 1000 events, we visualize only those with magnitude greater than 3ML. More detailed data for each window, with the percentage of events included into three intervals of

increasing magnitude and the corresponding final percentages of slightly damaged (P_{SDB}), heavily damaged (P_{HDB}) and destroyed (P_{DEB}) buildings, are reported below in Table 4.

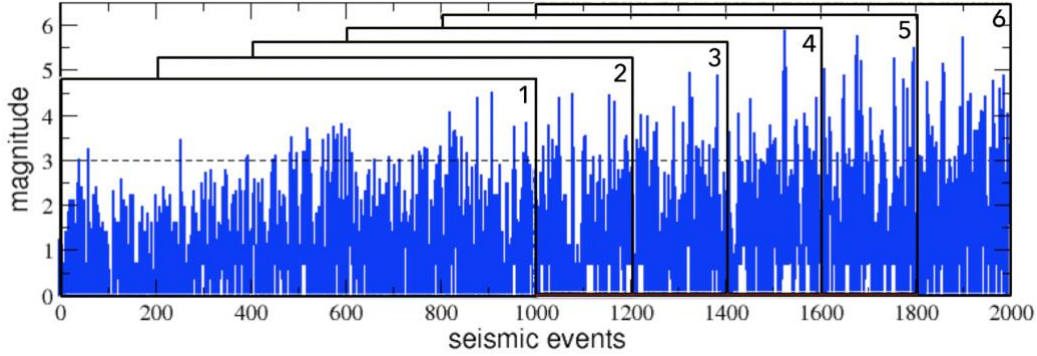


Figure 8. Complete sequence of 2000 events: a moving window of 1000 events progressively spans the sequence with steps of 200 events, then occupying six subsequent positions numbered from 1 to 6.

Table 4

WINDOW	EV $3 < M < 4$	EV $4 < M < 5$	EV $5 < M < 6$	P_{SDB}	P_{HDB}	P_{DEB}
1	3.9%	0.3%	0%	4.5%	0.7%	0%
2	5.2%	0.7%	0%	9.7%	6.8%	0.7%
3	6.8%	1.2%	0%	8.7%	27.3%	13.4%
4	7.1%	1.7%	0.2%	5.3%	24.0%	25.9%
5	7.3%	2.6%	0.7%	4.9%	15.6%	62.9%
6	8.5%	3.7%	0.9%	5.0%	9.9%	73.4%

Looking to the results, it is evident that – as expected – the damage scenario is strongly correlated with the seismic one, but this happens in a non-linear way: for example, a little increase in the percentage of seismic events with $4 < M < 5$ from window 2 (0.7%) to window 3 (1.2%) triggers a macroscopic jump in the percentage of highly damaged and destroyed buildings, which go – respectively – from 6.8% to 27.3% and from 0.7% to 13.4% (see Table 4). This is due to the intrinsic non-linear nature of three fundamental elements of the model, reflecting three important features present in the real world: the exponential increase of the energy released by an earthquake (represented by the number S of active sites in the OFC lattice) as function of its magnitude, the sigmoidal shape of the relation between seismic intensity and damage increment of a given building (governed by its actual vulnerability, see Eq.1), and the step-like function describing the change of status of the building (which depends on two subsequent thresholds in its total cumulated damage).

The combination of these elements makes also the simulated system – like all the real complex systems – very sensitive to its past seismic history, in the sense that two similar seismic events could have very different damage effects just because they happen in different moments. Look for example to window 5 in Figure 9: on one hand, the earthquake of 5.85ML occurred at the beginning of day 8th caused a sudden jump in the number of destroyed buildings from 1856 to 5335; on the other hand, the very similar

earthquake of 5.88ML, occurred at the end of day 9th, induced only a quite smaller increment of destroyed building, from 8025 to 8275.

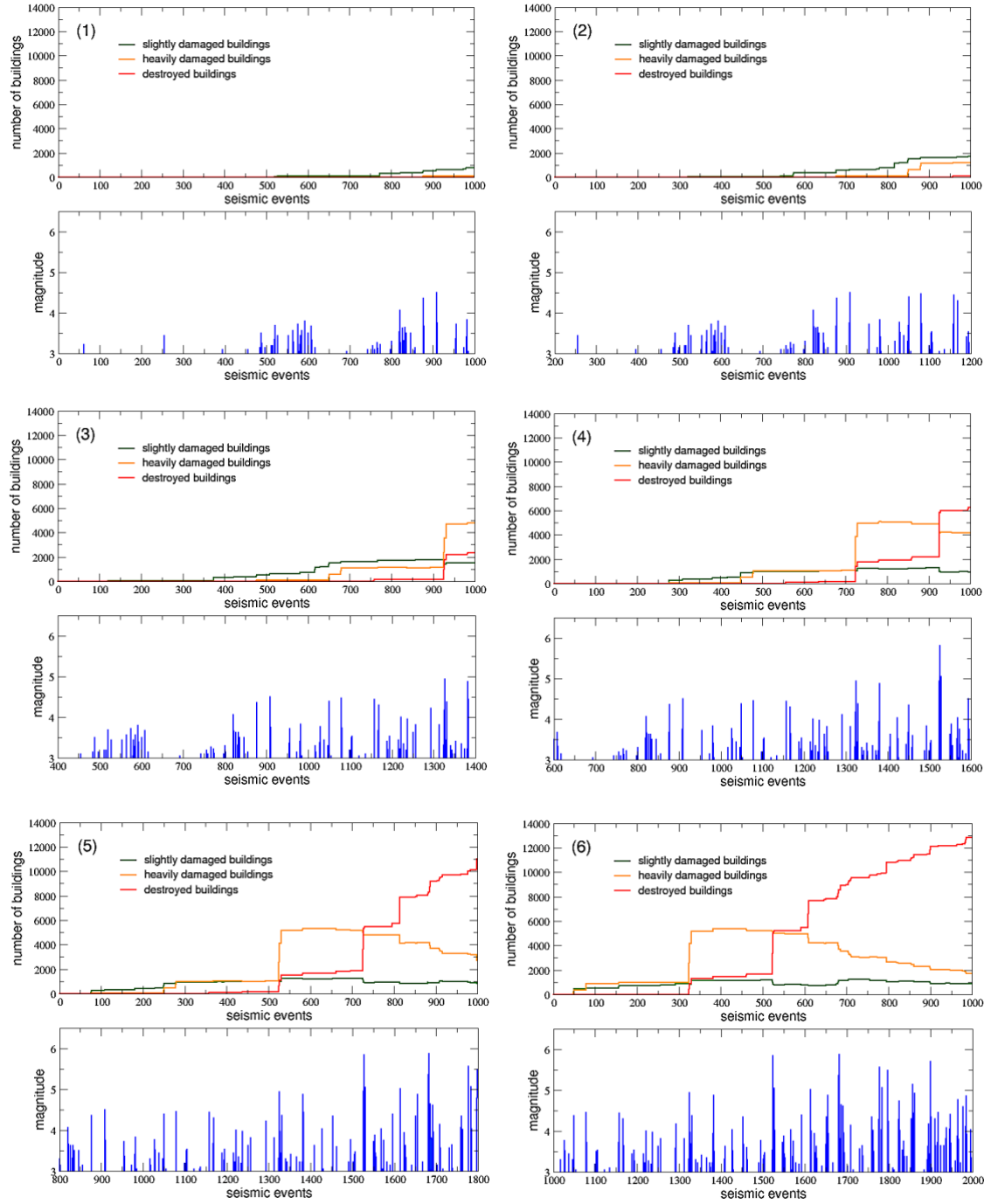


Figure 9. Top panels: for each one of the six subsequent positions of the moving window, the number of (slightly or heavily) damaged and destroyed buildings are reported as function of the 1000 seismic events included in the corresponding window; Bottom panels: the magnitude of the seismic events is reported for each position of the moving window.

In any case, it is clear that a large presence of the critical state into a given time window is essential in order to observe macroscopic damages. In fact, in windows 1, where the transient (of about 600 events, i.e. the first 6 days) covers 60% of the total time, leaving 40% only to the critical state (the last 4 days), the final percentage of highly damaged or destroyed buildings is practically zero. And only in the last three windows (4, 5 and 6), which are entirely inside the critical state, the final percentage of destroyed buildings exceeds 25%.

6.2 Analysis of damages as function of buildings' vulnerability

In this last subsection, we want to investigate the relationship between damages and some of the other buildings parameters in the context of a typical seismic scenario of duration 10 days inside the critical state (just after the usual transient of 600 events).

In Figure 10 the considered sequence of seismic events is plotted below the increase in the produced damages. Details about these plots are shown below, in Table 5.

Looking at Figure 10, one can notice that the main changes in the damage scenario do occur at days 6, 9 and 10, in correspondence of three important earthquakes of magnitude 4.77ML, 5.38ML and 5.04, respectively (see Table5). We report in Table 6 details about the percentages of slightly damaged (P_{SDB}), highly damaged (P_{HDB}), and destroyed (P_{DEB}) buildings as function of the percentage of events belonging to intervals of increasing magnitude. A comparison with the first day is also reported in the second column, while in the last row the geographical damage distributions are plotted day by day (undamaged buildings are coloured in dark green, slightly damaged in light green, heavily damaged in yellow and destroyed in red). The sudden increments in P_{HDB} at day 6 and the subsequent jumps in P_{DEB} at days 9 and 10 are clearly visible and can be also appreciated through the corresponding change of colours in the geographical distribution of damages.

Finally, in Table 7, a more detailed statistical analysis of the damage scenario at the end of the considered period of 10 days is presented. The percentage of increasing damage levels on the total amount of buildings is reported as function of some characteristic parameters. In particular, for each building, we consider its date of construction, the ratio H/L between the height of the building and the side length of its equivalent square plant, the initial vulnerability and the amplification level of the soil below the building.

The observation of the reported values show that the large majority of heavily damaged and destroyed buildings have been built before 1988. The influence of the ratio H/L on the presence of heavy damage or collapse is particularly significant in the range 0.5-2. The low values referred to ratios greater than 2 are related to the small presence of tall buildings in the considered area. With reference to the role of the initial vulnerability on the successive damage or collapse of the buildings, the results confirm that vulnerable structures are more prone to suffer severe damages. Finally, the greatest percentages of heavily damaged and destroyed building are located on soils with high values of the site amplification parameter.

The previous results show a satisfactory agreement with the expected damage scenarios for an urban area subjected to repetitive ground motions, thus further confirming the reliability of the proposed methodology. Of course, damage predictions could be improved by increasing the details provided by both the urban and geological GIS datasets.

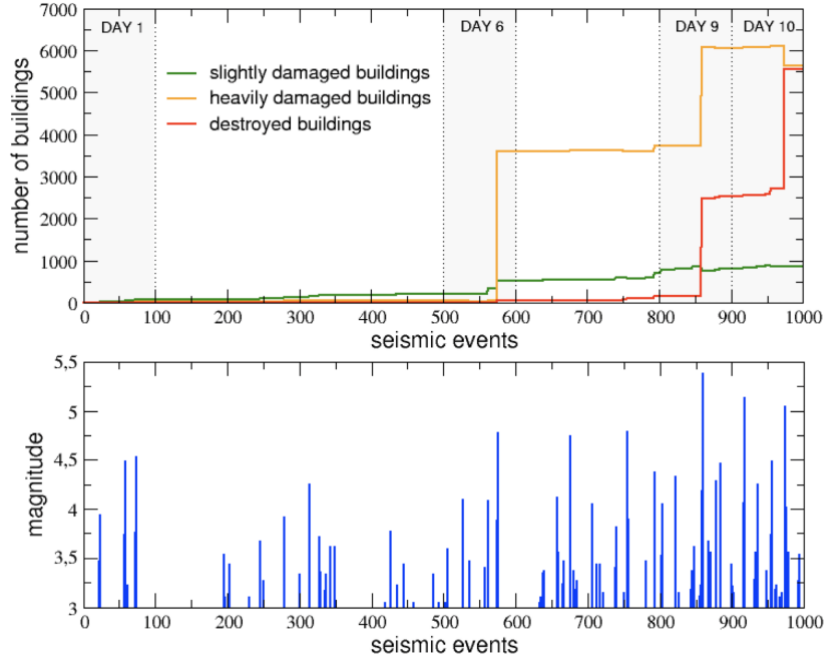


Figure 10. The number of (slightly or heavily) damaged and destroyed buildings are reported (top panel) as function of 1000 seismic events after a transient of 600 events (bottom panel). Only events with magnitude greater than 3ML are plotted.

Table 5

M = 3.93 EMS98 = 5.7 n-damaged = 0 n-destroyed = 0"	M = 3.04 EMS98 = 4.18 n-damaged = 39 n-destroyed = 9"	M = 4.04 EMS98 = 5.89 n-damaged = 3768 n-destroyed = 149"
M = 4.48 EMS98 = 6.63 n-damaged = 0 n-destroyed = 0"	M = 3.58 EMS98 = 5.1 n-damaged = 39 n-destroyed = 9"	M = 4.34 EMS98 = 6.4 n-damaged = 3763 n-destroyed = 154"
M = 3.22 EMS98 = 4.48 n-damaged = 0 n-destroyed = 0"	M = 4.09 EMS98 = 5.97 n-damaged = 39 n-destroyed = 9"	M = 3.14 EMS98 = 4.34 n-damaged = 3763 n-destroyed = 154"
M = 4.52 EMS98 = 6.7 n-damaged = 35 n-destroyed = 0"	M = 3.47 EMS98 = 4.9 n-damaged = 41 n-destroyed = 9"	M = 3.37 EMS98 = 4.73 n-damaged = 3763 n-destroyed = 154"
End Day 1	M = 3.4 EMS98 = 4.79 n-damaged = 41 n-destroyed = 9"	M = 3.61 EMS98 = 5.15 n-damaged = 3763 n-destroyed = 155"
M = 3.53 EMS98 = 5 n-damaged = 35 n-destroyed = 0"	M = 4.08 EMS98 = 5.94 n-damaged = 60 n-destroyed = 9"	M = 3.22 EMS98 = 4.48 n-damaged = 3763 n-destroyed = 156"
M = 3.09 EMS98 = 4.26 n-damaged = 35 n-destroyed = 0"	M = 4.77 EMS98 = 7.13 n-damaged = 3633 n-destroyed = 57"	M = 5.38 EMS98 = 8.16 n-damaged = 6112 n-destroyed = 2454"
End Day 2	End Day 6	M = 3.66 EMS98 = 5.24 n-damaged = 6110 n-destroyed = 2456"
M = 3.43 EMS98 = 4.85 n-damaged = 35 n-destroyed = 0"	M = 3.09 EMS98 = 4.26 n-damaged = 3633 n-destroyed = 57"	M = 3.53 EMS98 = 5 n-damaged = 6110 n-destroyed = 2456"
M = 3.09 EMS98 = 4.26 n-damaged = 35 n-destroyed = 0"	M = 3.33 EMS98 = 4.67 n-damaged = 3633 n-destroyed = 57"	M = 4.28 EMS98 = 6.29 n-damaged = 6106 n-destroyed = 2483"
M = 3.66 EMS98 = 5.24 n-damaged = 35 n-destroyed = 0"	M = 3.37 EMS98 = 4.73 n-damaged = 3633 n-destroyed = 57"	M = 4.45 EMS98 = 6.59 n-damaged = 6102 n-destroyed = 2514"
M = 3.26 EMS98 = 4.54 n-damaged = 35 n-destroyed = 0"	M = 4.11 EMS98 = 6 n-damaged = 3634 n-destroyed = 59"	End Day 9
M = 3.91 EMS98 = 5.66 n-damaged = 40 n-destroyed = 0"	M = 3.47 EMS98 = 4.9 n-damaged = 3634 n-destroyed = 59"	M = 3.43 EMS98 = 4.85 n-damaged = 6101 n-destroyed = 2515"
End Day 3	M = 4.74 EMS98 = 7.09 n-damaged = 3651 n-destroyed = 60"	M = 3.14 EMS98 = 4.34 n-damaged = 6101 n-destroyed = 2515"
M = 3.33 EMS98 = 4.67 n-damaged = 40 n-destroyed = 0"	M = 3.37 EMS98 = 4.73 n-damaged = 3651 n-destroyed = 60"	M = 5.11 EMS98 = 7.71 n-damaged = 6115 n-destroyed = 2538"
M = 4.25 EMS98 = 6.24 n-damaged = 40 n-destroyed = 0"	M = 3.26 EMS98 = 4.54 n-damaged = 3651 n-destroyed = 60"	M = 3.61 EMS98 = 5.15 n-damaged = 6115 n-destroyed = 2538"
M = 3.71 EMS98 = 5.32 n-damaged = 39 n-destroyed = 9"	End Day 7	M = 4.26 EMS98 = 6.26 n-damaged = 6116 n-destroyed = 2541"
M = 3.33 EMS98 = 4.67 n-damaged = 39 n-destroyed = 9"	M = 4.04 EMS98 = 5.89 n-damaged = 3653 n-destroyed = 60"	M = 3.37 EMS98 = 4.73 n-damaged = 6113 n-destroyed = 2544"
M = 3.61 EMS98 = 5.15 n-damaged = 39 n-destroyed = 9"	M = 3.43 EMS98 = 4.85 n-damaged = 3651 n-destroyed = 62"	M = 4.48 EMS98 = 6.63 n-damaged = 6154 n-destroyed = 2694"
End Day 4	M = 3.43 EMS98 = 4.85 n-damaged = 3651 n-destroyed = 62"	M = 3.14 EMS98 = 4.34 n-damaged = 6154 n-destroyed = 2694"
M = 3.04 EMS98 = 4.18 n-damaged = 39 n-destroyed = 9"	M = 3.14 EMS98 = 4.34 n-damaged = 3651 n-destroyed = 62"	M = 3.22 EMS98 = 4.48 n-damaged = 6154 n-destroyed = 2694"
M = 3.76 EMS98 = 5.4 n-damaged = 39 n-destroyed = 9"	M = 3.76 EMS98 = 5.4 n-damaged = 3652 n-destroyed = 62"	M = 3.09 EMS98 = 4.26 n-damaged = 6155 n-destroyed = 2694"
M = 3.22 EMS98 = 4.48 n-damaged = 39 n-destroyed = 9"	M = 3.71 EMS98 = 5.32 n-damaged = 3653 n-destroyed = 62"	M = 3.22 EMS98 = 4.48 n-damaged = 6155 n-destroyed = 2694"
M = 3.43 EMS98 = 4.85 n-damaged = 39 n-destroyed = 9"	M = 3.14 EMS98 = 4.34 n-damaged = 3626 n-destroyed = 90"	M = 5.04 EMS98 = 7.58 n-damaged = 5601 n-destroyed = 5550"
M = 3.04 EMS98 = 4.18 n-damaged = 39 n-destroyed = 9"	M = 4.78 EMS98 = 7.14 n-damaged = 3639 n-destroyed = 102"	M = 3.56 EMS98 = 5.05 n-damaged = 5600 n-destroyed = 5553"
M = 3.33 EMS98 = 4.67 n-damaged = 39 n-destroyed = 9"	M = 3.47 EMS98 = 4.9 n-damaged = 3638 n-destroyed = 103"	M = 3.53 EMS98 = 5 n-damaged = 5600 n-destroyed = 5553"
M = 3.04 EMS98 = 4.18 n-damaged = 39 n-destroyed = 9"	M = 4.37 EMS98 = 6.44 n-damaged = 3755 n-destroyed = 148"	End Day 10
End Day 5	End Day 8	M = 3.43 EMS98 = 4.85 n-damaged = 6101 n-destroyed = 2515"
M = 3.04 EMS98 = 4.18 n-damaged = 39 n-destroyed = 9"	M = 3.14 EMS98 = 4.34 n-damaged = 3626 n-destroyed = 90"	M = 5.11 EMS98 = 7.71 n-damaged = 6115 n-destroyed = 2538"
M = 3.76 EMS98 = 5.4 n-damaged = 39 n-destroyed = 9"	M = 4.78 EMS98 = 7.14 n-damaged = 3639 n-destroyed = 102"	M = 3.61 EMS98 = 5.15 n-damaged = 6115 n-destroyed = 2538"
M = 3.22 EMS98 = 4.48 n-damaged = 39 n-destroyed = 9"	M = 3.47 EMS98 = 4.9 n-damaged = 3638 n-destroyed = 103"	M = 4.26 EMS98 = 6.26 n-damaged = 6116 n-destroyed = 2541"
M = 3.43 EMS98 = 4.85 n-damaged = 39 n-destroyed = 9"	M = 4.37 EMS98 = 6.44 n-damaged = 3755 n-destroyed = 148"	M = 3.37 EMS98 = 4.73 n-damaged = 6113 n-destroyed = 2544"
M = 3.04 EMS98 = 4.18 n-damaged = 39 n-destroyed = 9"		M = 4.48 EMS98 = 6.63 n-damaged = 6154 n-destroyed = 2694"
M = 3.33 EMS98 = 4.67 n-damaged = 39 n-destroyed = 9"		M = 3.14 EMS98 = 4.34 n-damaged = 6154 n-destroyed = 2694"
M = 3.04 EMS98 = 4.18 n-damaged = 39 n-destroyed = 9"		M = 3.22 EMS98 = 4.48 n-damaged = 6154 n-destroyed = 2694"
		M = 3.09 EMS98 = 4.26 n-damaged = 6155 n-destroyed = 2694"
		M = 3.22 EMS98 = 4.48 n-damaged = 6155 n-destroyed = 2694"
		M = 5.04 EMS98 = 7.58 n-damaged = 5601 n-destroyed = 5550"
		M = 3.56 EMS98 = 5.05 n-damaged = 5600 n-destroyed = 5553"
		M = 3.53 EMS98 = 5 n-damaged = 5600 n-destroyed = 5553"
		End Day 10

Table 6





DAY	1	6	9	10
EV $3 < M < 4$	2%	25%	44%	54.5%
EV $4 < M < 5$	2%	6%	15%	17.2%
EV $5 < M < 6$	0%	0%	1%	3%
P _{SDB}	0.4%	3.0%	4.7%	4.9%
P _{HDB}	0.2%	20.6%	34.5%	32.2%
P _{DEB}	0%	0.3%	14.5%	31.8%
Geographical Damage Distribution				

Table 7

Parameter		%Undamaged buildings	%Slightly damaged buildings	%Highly damaged buildings	%Destroyed buildings
Date of construction	1912 - 1940	7.7	0.1	14.1	13.7
	1941 - 1964	3.3	0.2	5.3	5.6
	1965 - 1987	15.1	3.6	12.7	11.2
	1988 - 1999	1.5	0.3	0.6	0.5
	2000 - 2007	0.2	0.6	0.2	0.1
	2008 - 2018	3.5	0	0.7	0.7
Ratio H/L	<0.5	12.2	2.6	5.1	4.7
	0.5-2	17.8	2.1	24.8	24.3
	>2	1.4	0	2.2	2.9
Initial vulnerability	low	3.1	0.5	0.7	0.5
	medium	14.2	3	10	9.3
	high	14.0	1.3	21.4	22
Site amplification	medium-low	3.5	1.8	0.7	0.9
	medium	5.2	0.6	1.5	1.0
	high	22.6	2.4	29.8	29.9

7. Conclusions

This study represents a first attempt to apply a new multidisciplinary agent-based approach to the seismic assessment of a large urban, and peri-urban, area. By integrating competences and information coming from several scientific disciplines, going from the SOC dynamics of earthquakes to the seismic response of buildings with a given vulnerability, from the GIS features of the urban settlement to agent-based simulations, the proposed methodology allows to evaluate the effects of long sequences of seismic shocks, with representative power-law distributed intensities on the buildings present in the area under

investigation, assuming that the latter is in a critical state. In the paper, a small portion of the territory of Avola (Siracusa, Italy) has been considered as a case study. The similarity, from the point of view of the seismic risk, of this area with the one involved in the earthquake occurred in L'Aquila in 2009 allowed us to calibrate the model with real data, even though referred to a similar territory. Then, several damage scenarios related to new possible repetitive earthquakes have been considered. The numerical results clearly show the potentialities of the present approach. It is worth noting, in the application here reported, that the proposed methodology has been applied to the scale of a small town for investigating the distribution of damages at the detail level of a single building. Therefore, on one hand, the reliability of the obtained results could encourage forward-looking municipal administrations to adopt this kind of tool in order to implement both prevention and emergency plans concerning the related urban territory. On the other hand, such an approach could also be easily extended to a larger scale in order to address the seismic vulnerability of several homogeneous urban areas interested by common seismogenetic sources. For example, one could consider the case of the Oriental Sicily area, whose seismic risk is mainly associated to the Ibleo-Maltese system of faults that were responsible of the great devastating 1963 earthquake. Finally this tool could also be used to investigate how to increase the resilience of urban areas, or in reducing the seismic vulnerability, by improving the structural performance of the most vulnerable buildings, through ad hoc retrofitting strategies, or planning new safety areas that could diminish the risk for the population living there or even implementing more efficient and timely evacuation plans in case of small but repeated seismic events that could put at risk the population.

References

- [1] Ramos L.F, Lourenço P.B. Modelling and vulnerability of historical city centres in seismic areas: a case study in Lisbon. *Engineering Structures* (2004) **26**(9): 1295-1310.
- [2] Maio R, Vicente R, Formisano A, Varum H. Seismic vulnerability of building aggregates through hybrid and indirect assessment techniques. *Bulletin of Earthquake Engineering* (2015) **13**(10): 2995-3014.
- [3] Maio R, Ferreira T. M, Vicente R. A critical discussion on the earthquake risk mitigation of urban cultural heritage assets. *International Journal of Disaster Risk Reduction* (2016) **27**: 239-247.
- [4] Senaldi I, Magenes G, Penna A. Numerical investigations on the seismic response of masonry building aggregates. *Advanced Materials Research* (2010) **133**:715-720.
- [5] Greco A, Lombardo G, Pantò B, Famà A. Seismic vulnerability of historical masonry aggregate buildings in oriental Sicily. *International Journal of Architectural Heritage* (2018) DOI: 10.1080/15583058.2018.1553075
- [6] Di Pasquale G, Orsini G, A Pugliese, Romeo RW. Damage scenario for future earthquakes. In: proceedings of the 11th European conference on earthquake engineering, Paris; 1998.
- [7] Omori, F. On the aftershocks of earthquakes". *Journal of the College of Science, Imperial University of Tokyo*. (1894). 7: 111–200.
- [8] Utsu, T.; Ogata, Y.; Matsu'ura, R.S. The centenary of the Omori formula for a decay law of aftershock activity" *Journal of Physics of the Earth*. (1995) 43: 1–33.

- [9] Watts D.J., Strogatz S.H., Collective dynamics of ‘small-world’ networks, *Nature* (1998) 393, 440
- [10] Bak P, Tang C and Wiesenfeld K. Self-organized criticality: An explanation of the 1/f noise. *Phys. Rev. Lett.* **59**, 381, 1987
- [11] Jensen HJ. Self-Organized Criticality: Emergent Complex Behavior in Physical and Biological Systems. Cambridge Lecture Notes in Physics, 1998.
- [12] Olami Z, Feder HJS, Christensen K. Self-organized criticality in a continuous, nonconservative cellular automaton modeling earthquakes. *Phys Rev E* 1992; **68**(8):1244–1247
- [13] EMS. European Macroseismic Scale, 1998. Conseil de l'Europe. European Seism. Commission. 8 LUXEMBOURG 1998.
- [14] Carocci, C.F. Small centres damaged by 2009 L'Aquila earthquake: On site analyses of historical masonry aggregates, *Bulletin of Earthquake Engineering* (2012) **10**: 45-71.
- [15] Kawashima K, Aydan O, Aoki T, Kisimoto I, Konagai K, Matsui T, Sakuta J, Takahashi N, Teodori S, Yashima A. Reconnaissance investigation on the damage of The 2009 L'Aquila, central Italy earthquake, *Journal of Earthquake Engineering*, (2010) **14**:816-841.
- [16] Decanini L.D, Liberatore L, Mollaioli F. Damage potential of the 2009 L'Aquila, Italy, earthquake. *Journal of Earthquake and Tsunami* (2012) **6**(3)
- [17] Bosi A, Marazzi F, Pinto A, Tsionis G. The L'Aquila (Italy) earthquake of 6 April 2009: report and analysis from a field mission. Scientific and Technical Research Reports, Publications Office of the European Union 978-92-79-18990-6 (2011)
- [18] Lagomarsino S, Giovinazzi S. Macroseismic and mechanical models for the vulnerability and damage assessment of current buildings. *Bull Earthquake Eng* 2006; **4**:415–443.
- [19] Polese M, Di Ludovico M, Prota A, Manfredi G. Damage-dependent vulnerability curves for existing buildings. *Earthquake Engineering and Structural Dynamics* (2013) **42**:853–870
- [20] Zuccaro G, Cacace F. Seismic vulnerability assessment based on typological characteristics. The first level procedure “SAVE”. *Soil Dynamics and Earthquake Engineering* 2015; **69**:262–269.
- [21] Musson R.M.W., Gruntal G, Stucchi M., The comparison of macroseismic intensity scales, *Journal of Seismology* (2010) **14**: 413-428
- [22] Caruso F, Pluchino A, Latora V, Vinciguerra S, Rapisarda A. A new analysis of Self-Organized Criticality in the OFC model and in real earthquakes. *Phys Rev E* **75** (2007) 055101(R)
- [23] Barbarossa L, Privitera R, Martinico F. Insediamenti irregolari e rischi territoriali lungo i litorali del Val di Noto. Percorsi di progetto per la città costiera resiliente. Atti della XIX Conferenza sui Cambiamenti, Catania 16 -18 giugno 2016. Planum Publisher, 2016